

# CUL-2 is required for the G1-to-S-phase transition and mitotic chromosome condensation in *Caenorhabditis elegans*

Hui Feng\* †, Weiwei Zhong\* †, George Punkosdy\*, Subin Gu\*, Liang Zhou\*, Erin K. Seabolt\* and Edward T. Kipreos\* ‡

\*Department of Cellular Biology, University of Georgia, Athens, Georgia 30602, USA

‡e-mail: ekipreos@cb.uga.edu

†These authors contributed equally to this work

**The human cullin protein CUL-2 functions in a ubiquitin-ligase complex with the von Hippel-Lindau (VHL) tumour suppressor protein. Here we show that, in *Caenorhabditis elegans*, *cul-2* is expressed in proliferating cells and is required at two distinct points in the cell cycle, the G1-to-S-phase transition and mitosis. *cul-2* mutant germ cells undergo a G1-phase arrest that correlates with accumulation of CKI-1, a member of the CIP/KIP family of cyclin-dependent-kinase inhibitors. In *cul-2* mutant embryos, mitotic chromosomes are unable to condense, leading to unequal DNA segregation, chromosome bridging and the formation of multiple nuclei.**

Eukaryotic cell-cycle transitions are regulated in large part by the activity of cyclin-dependent kinases (CDKs). CDKs are regulated by phosphorylation and by association with activating cyclins and inhibitory CDK inhibitors (CKIs)<sup>1</sup>. The transition from one cell-cycle state to another is made irreversible by the ubiquitin-mediated degradation of cyclins and CKIs. The specificity of ubiquitin-mediated degradation is determined by ubiquitin-conjugating enzymes, E2s, which transfer ubiquitin to substrates, and ubiquitin ligases, E3s, which act as conduits to bring the E2 to the substrate<sup>2</sup>. There are two classes of E3 complex that have been implicated in cell-cycle control: the anaphase-promoting complex (APC) or cyclosome, which is required for the metaphase-to-anaphase transition and for exit from mitosis, and SCF complexes, which are required for transitions from both G1 to S phase and G2 to M phase<sup>3–6</sup>.

SCF complexes are composed of Skp1, cullin, an F-box protein and Rbx1/Roc1 proteins<sup>7–12</sup>. The cullin protein links the E2 to the E3 complex, which recognizes the substrate<sup>7,8</sup>. In *Saccharomyces cerevisiae*, the cullin Cdc53 functions in at least three distinct SCF complexes that target the degradation of metabolic regulatory factors, as well as both positive and negative cell-cycle regulators, namely G1 cyclins (Cln1 and Cln2), CKIs (Far1 and Sic1), and the CDK-inhibitory kinase Swe1 (refs 5–8, 13–16).

In higher eukaryotes, the cullin family encompasses six genes in humans and in *C. elegans*<sup>17</sup> (data not shown). The human CUL-2 protein has been found in a complex containing the VHL tumour suppressor protein, Elongin-C (a Skp1 homologue), Elongin-B (a ubiquitin-like protein), and RBX1/ROC1 (refs 9, 18, 19). The CUL-2–VCB complex possesses ubiquitin-ligase activity *in vitro*, which is lost in tumour-derived VHL mutants<sup>20</sup>. VHL binds hypoxia-inducible transcription factors and facilitates their degradation<sup>21</sup>. However, the mechanism of VHL-mediated tumour suppression remains unclear<sup>22</sup>.

Here we report that *C. elegans* CUL-2 functions as a positive cell-cycle regulator. In the absence of *cul-2*, germ cells undergo G1-phase arrest, which correlates with a post-transcriptional accumulation of CKI-1, a member of the CIP/KIP family of CKIs. Surprisingly, *cul-2* is also required for mitotic chromosome condensation.

## Results

***cul-2* developmental expression.** We determined the developmental expression of *cul-2* messenger RNA by *in situ* hybridization. In

adults, the major site of *cul-2* mRNA expression is the germ line (Fig. 1a, b). *cul-2* mRNA is provided to embryos as maternal product, and during embryogenesis the levels of *cul-2* mRNA decrease (Fig. 1f, g). During larval development, *cul-2* mRNA is found in proliferating tissues, with the highest level in the intestine, which endoreplicates at each larval molt<sup>23</sup>, as well as in a few postmitotic neurons in the nerve ring (Fig. 1c–e).

To determine the CUL-2 protein expression pattern, we generated anti-CUL-2 antibodies. In adults, CUL-2 is observed in the germ line, with higher levels in meiotic cells (data not shown). The highest CUL-2 levels are found in oocytes, where CUL-2 is mainly nuclear with some cytoplasmic staining (Fig. 1j–k). Disruption of *cul-2* expression by double-stranded RNA-mediated interference (RNAi)<sup>24</sup> severely reduces the levels of both nuclear and cytoplasmic anti-CUL-2 staining (Fig. 1l, m). Similar to *cul-2* mRNA, CUL-2 protein is provided to embryos as maternal product and the level decreases during embryogenesis (Fig. 1h, i). During larval development, CUL-2 is found in the following proliferating tissues: P cells during the L1 stage (data not shown); seam cells when they divide at every molt (Fig. 1o, p); vulval and somatic gonad cells in late L3 and L4 stages (Fig. 1n); and intestinal cells throughout larval development (Fig. 1n).

**Isolation of a *cul-2* deletion mutant.** We recovered a single *cul-2* allele, *ek1*, after screening a 370,000-genome deletion library. The *ek1* mutation is a 1.2-kilobase deletion that removes exons 2, 3 and 4, as well as the 5' splice site of exon 5 (Fig. 2). The mutant allele is completely recessive. *cul-2* homozygous progeny of heterozygous parents have normal embryonic and postembryonic somatic cell divisions (data not shown).

**G1 arrest of *cul-2* germ cells.** Beginning in the L3 stage, *cul-2(ek1)* mutants have fewer germ cells than wild-type animals (Fig. 3c). At 61 h post-hatching, adult *cul-2* homozygotes have on average 270 germ cells, whereas *cul-2* heterozygotes have 1,040 germ cells (Fig. 3c). *cul-2* germ-cell nuclei are twofold larger than wild-type nuclei at the L4 stage ( $54 \pm 16 \mu\text{m}^3$  versus  $27 \pm 6.1 \mu\text{m}^3$ , respectively;  $n = 30$ ; Fig. 3a, b).

To determine whether the *cul-2* phenotype of fewer, larger germ cells was due to a G1 arrest or endoreplication, we measured the genomic DNA content of germ cells in *cul-2(ek1)* homozygotes and wild-type animals. Wild-type germ cells have a bimodal distribution, with most of the cells having either a 2N or a 4N DNA content, corresponding to G1 and G2/M phases, respectively (Fig. 3d). In contrast, *cul-2* mutants have a single peak at 2N, indicating that *cul-*

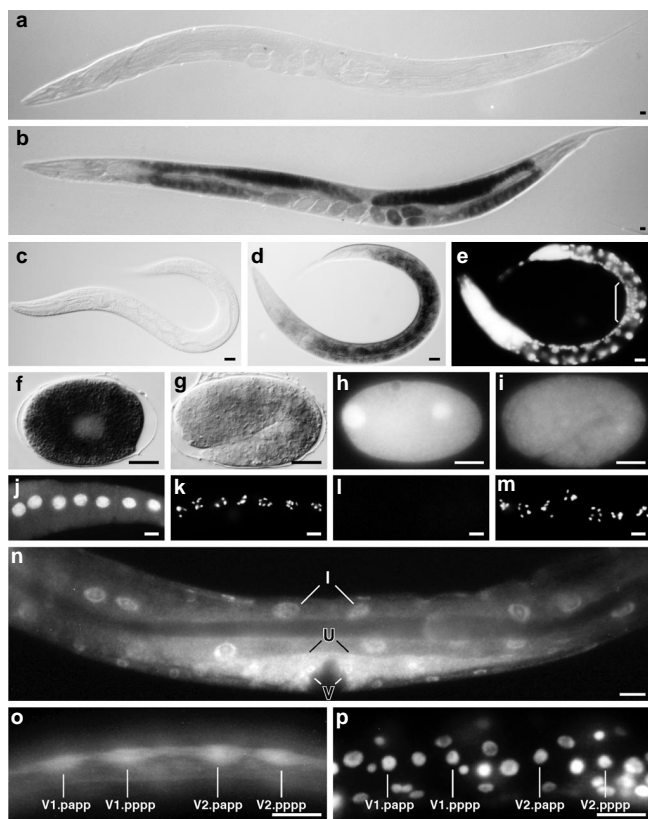


**Figure 1 Developmental expression of *cul-2*.** **a, b**, *In situ* hybridization of adult wild-type hermaphrodites with control *cul-2* sense RNA (**a**) or *cul-2* antisense RNA (**b**). **c, d**, *In situ* hybridization of L2-stage larvae with *cul-2* sense RNA (**c**) or *cul-2* antisense RNA (**d**). **e**, DAPI stain of the L2 larvae shown in **d**. Bracket denotes the longitudinal extent of the gonad. **f, g**, *In situ* hybridization of a zygote (**f**) and twofold-stage embryo (**g**) with *cul-2* antisense RNA. **h, i**, A zygote with two pronuclei (**h**) and a 1.5-fold-stage embryo (**i**) stained with anti-CUL-2 antibody. **j, k**, Wild-type oocytes co-stained with anti-CUL-2 antibody (**j**) and DAPI (**k**). **l, m**, Oocytes from wild-type hermaphrodites that were injected with *cul-2* dsRNA are co-stained with anti-CUL-2 antibody (**l**) and DAPI (**m**). Proximal oocytes are to the left. **n**, L4-stage hermaphrodite stained with anti-CUL-2 antibody. V, U and I denote vulva, uterus and intestinal nuclei, respectively. **o, p**, Lateral hypodermis of early L3-stage larvae co-stained with anti-CUL-2 antibody (**o**) and DAPI (**p**). Seam cells (marked) have high levels of CUL-2 at the molt. Anterior is to the left. Scale bars represent 10 μm.

2 germ cells undergo a G1-phase arrest with cells either severely delayed or blocked in entry into S phase.

**Accumulation of CKI-1 in *cul-2* mutants.** The finding that *cul-2* mutant germ cells undergo a G1 arrest, coupled with the fact that the cullin Cdc53 functions to degrade CKIs, raised the possibility that CUL-2 also functions to degrade CKIs. To address this possibility, we identified two *CIP/KIP* homologues in the *C. elegans* genome, *cki-1* and *cki-2* (Fig. 4a–c).

Inactivation of *cki-2* by RNAi produces an impenetrant embryonic-arrest phenotype. About 10% of *cki-2* RNAi embryos arrest development with 242 ± 51 cells (*n* = 13), which is less than the wild-type cell number at hatch (558 cells). No larval mutant phenotypes were observed in the *cki-2* RNAi animals that hatched. *cki-1* RNAi produces a low penetrance of embryos that arrested with hyperplasia (>750 cells per embryo) and a high penetrance of larval hyperplasia of the somatic gonad, vulva and hypodermis (Fig. 4d–f and data not shown), indicating that *cki-1* functions as a negative cell-cycle regulator. While our project was under way, Hong *et al.* reported similar *cki-1* RNAi results<sup>25</sup>.

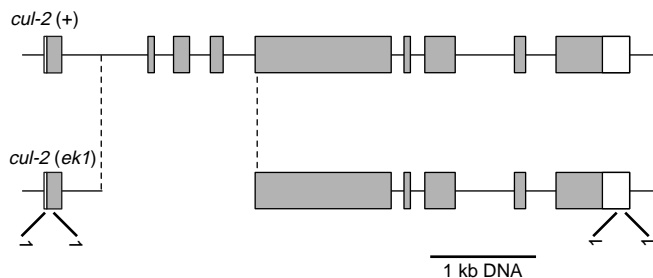


**Figure 2 *cul-2* deletion mutant.** Line drawing of the *cul-2* genomic region on chromosome III, with exons represented as boxes and introns as horizontal lines. Shaded areas represent coding regions. The cDNA sequence of *cul-2* was from ref. 17, and the genomic sequence is from cosmid ZK520 (GenBank accession number Z92822). The region deleted in *cul-2(ek1)* is represented as the missing region bounded by dashed lines, and includes exons 2–4 as well as the first four base pairs of exon 5. The deletion includes base pairs 12,166–13,393 of cosmid ZK520. Locations of primers used for the deletion screen are shown below the genomic line drawing as half-arrows. kb, kilobase.

To determine whether the level of CKI-1 was increased in *cul-2* germ cells, we generated anti-CKI-1 antibodies (Fig. 5a–d). In the distal mitotic germ cells of wild-type animals, the amount of CKI-1 is low. As germ cells enter meiosis, the level of CKI-1 increases, with the highest intensity being observed in oocyte nuclei (Fig. 5e, g). In *cul-2(ek1)* gonad arms, the level of CKI-1 is higher, particularly in the distal region (Fig. 5f, h). The amount of anti-CKI-1 signal per distal nucleus in *cul-2(ek1)* gonads is 13-fold higher than in the wild type (13 ± 10 arbitrary units (a.u.), *n* = 50, versus 1.0 ± 0.9 a.u., *n* = 36). In contrast, the *cki-1* mRNA *in situ* signal in *cul-2* gonads is lower than in the wild type (1.0 ± 0.5 a.u., *n* = 8, versus 2.1 ± 0.7 a.u., *n* = 10, respectively) (Fig. 5i–k). We also produced affinity-purified antibodies to the CKI-2 protein. We did not observe an increase in CKI-2 protein in *cul-2* gonads (data not shown).

**Suppression of the *cul-2* G1 arrest.** If the increased level of CKI-1 protein in germ cells were contributing to the G1 arrest, then reducing the level of CKI-1 should suppress the phenotype. To test this possibility, we created the strain *cul-2(ek1)/unc-64(e246); mnDf100 unc-4(e120)/mnC1*, in which one chromosomal copy of *cki-1/-2* was deleted by the deficiency *mnDf100*. In this strain, germ-cell number is increased by 30% in comparison with *cul-2(ek1)* animals (353 ± 25 cells versus 278 ± 59 cells, *n* = 11, respectively). This increased cell number correlates with a 3.3-fold higher egg number (57 ± 18 eggs versus 17 ± 13 eggs, *n* = 22), indicating a partial suppression of the *cul-2* germ-cell arrest. Introducing T05A6, a cosmid containing *cki-1* and *cki-2*, into this strain abolishes the suppression (15 ± 20 eggs, *n* = 22). To distinguish the roles of *cki-1* and *cki-2* in the suppression of *cul-2*, we injected double-stranded RNA encoding either gene into L4-stage *cul-2* hermaphrodites and then determined the number of eggs produced as adults. *cki-1* RNAi is capable of partially suppressing the *cul-2* arrest (58 ± 21 eggs, *n* = 10). In contrast, *cki-2* RNAi does not suppress the germ-cell arrest (15 ± 26 eggs, *n* = 11). Injection of either *cki-1* or *cki-2* dsRNA into wild-type animals does not increase egg number (data not shown).

***cul-1* and *cul-2* are not functionally redundant.** *cul-1* is the closest paralogue of *cul-2* (ref. 17). In contrast to the *cul-2* G1-arrest phenotype, *cul-1* mutants show hyperplasia of blast-cell lineages<sup>17</sup>. We observed no increase in the level of CKI-1 in *cul-1* mutants (data not shown). To explore the possibility of redundancy of function between *cul-1* and *cul-2*, we created a double heterozygous strain with *cul-1(e1756)* and *cul-2(ek1)*. The germ cells of *cul-1, cul-2* double homozygotes arrest in G1, with a phenotype and CKI-1 level identical to those of *cul-2(ek1)* germ cells (data not shown). The larval somatic blast cells of *cul-1, cul-2* double homozygotes show hyperplasia, although this is less severe than that in *cul-1* mutants

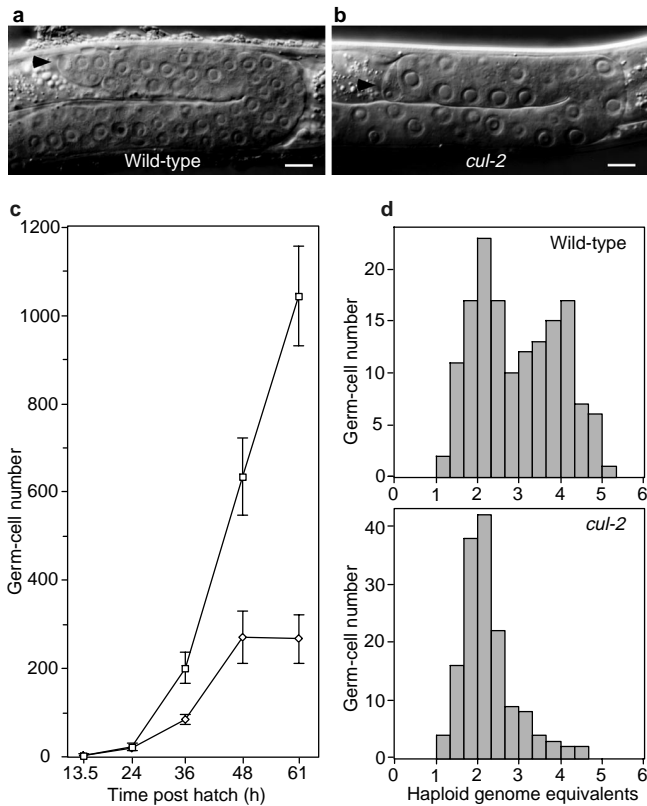


**Figure 3 G1 arrest of *cul-2* germ cells.** **a, b**, Differential-interference contrast (DIC) micrographs of the distal gonad arms of wild-type **(a)** and *cul-2*(*ek1*) **(b)** L4-stage hermaphrodites. The distal tip cell is denoted by an arrow. Scale bars represent 10 μm. **c**, Hermaphrodite germ-cell number in *cul-2*(*ek1*) homozygotes (diamonds) and *cul-2*(*ek1*)/*unc-64*(*e264*) heterozygotes (squares) grown at 20 °C for the following hours post hatching: 13.5 h (L1 stage); 24 h (L2 stage); 36 h (young L4 stage); 48 h (young adult); and 61 h (mature adult). **d**, Histogram of DNA content of germ cells from young adult *cul-2*(*ek1*) and wild-type hermaphrodites.

alone (L4 *cul-1*, *cul-2* mutants had 53 ± 8 vulval cells, *n* = 11, versus 82 ± 16 vulval cells, *n* = 20, in *cul-1* mutants; ref. 17). These observations indicate that there is no significant functional redundancy between the two genes and that the *cul-2* G1-arrest phenotype is epistatic to the *cul-1* hyperplasia phenotype.

**Embryonic *cul-2* phenotype.** *cul-2* embryos laid by *cul-2* homozygotes arrest development at a very early stage with only 24 ± 4.6 cells, *n* = 20 (Fig. 6i). This arrest does not appear to be due to CKI-1 accumulation, as the level of CKI-1 in *cul-2* embryos is the same as that in wild-type embryos (data not shown). CKI-1 protein is maternally provided and does not appear to inhibit the rapid cell divisions of the early embryo (data not shown). Substrates of SCF E3 complexes are known to be targeted for ubiquitination by phosphorylation<sup>3</sup>, and it is, therefore, possible that the maternal CKI-1 is not marked (by phosphorylation) for degradation.

*cul-2* homozygotes from heterozygous parents show normal development, whereas *cul-2* RNAi produces 100% arrested embryos in the immediate progeny. This result indicates that the *cul-2* maternal product may be sufficient to allow normal embryonic development.

Early meiotic events, before fertilization, appear to be normal in *cul-2* mutants. Equal segregation of genomic DNA occurs in meiosis I in 4 out of 4 observed embryos. However, only one-third of *cul-2* zygotes show normal meiosis II (6 out of 18), with the remainder failing to extrude a second polar body or having an abnormal DNA distribution.

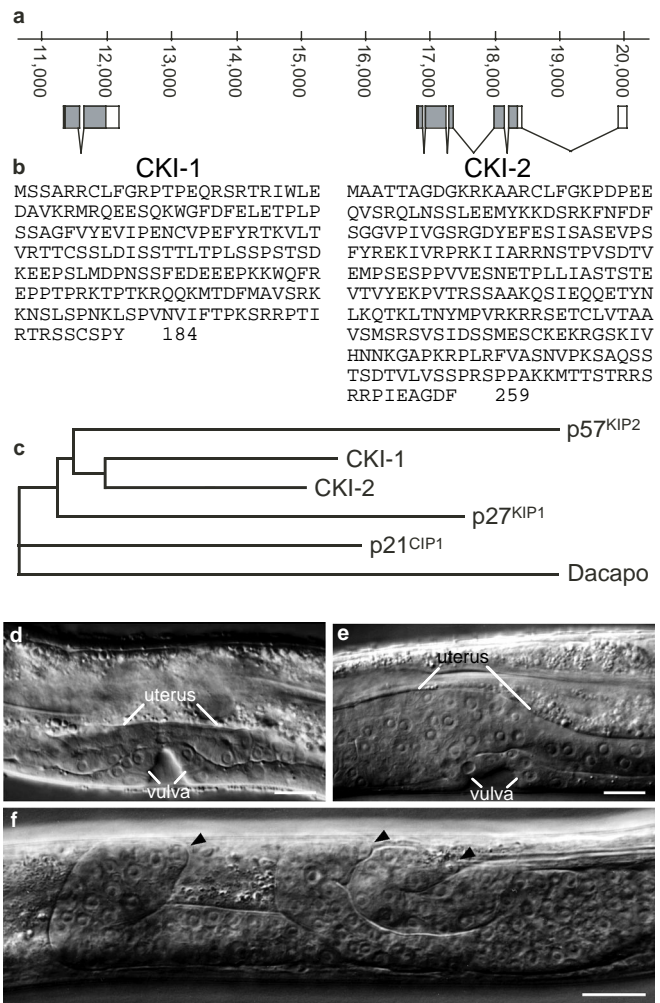


**Figure 4 *cki-1* and *cki-2* cloning and RNAi phenotype.** **a**, Location of *cki-1* and *cki-2* in a 9-kilobase region of cosmid T05A6. Exons are presented as boxes and coding regions are shaded. *cki-1* corresponds to gene T05A6.1 and *cki-2* corresponds to T05A6.2. **b**, The predicted protein sequences from the *cki-1* and *cki-2* cDNAs. *cki-1* and *cki-2* share 21–27% sequence identity with mammalian p21<sup>CIP1</sup> and p27<sup>KIP1</sup>, and share 26% identity between themselves. **c**, Phylogram of CKI proteins from *C. elegans* (CKI-1 and CKI-2), *Homo sapiens* (p21<sup>CIP1</sup>, p27<sup>KIP1</sup> and p57<sup>KIP2</sup>), and *Drosophila melanogaster* (Dacapo), showing the most parsimonious tree. **d, e**, Uterine hyperplasia is induced by *cki-1* RNAi. Differential-interference contrast (DIC) micrograph of the vulva and uterus of **d**, an L4-stage progeny from an uninjected wild-type hermaphrodite, and **e**, an L4-stage progeny from a wild-type hermaphrodite injected with *cki-1* dsRNA. **f**, Extra distal tip cells produce extra gonad arms in *cki-1* RNAi progeny. DIC micrograph of anterior gonads of an L4-stage progeny of a wild-type hermaphrodite injected with *cki-1* dsRNA. Distal tip cells, which direct the migration of the developing gonad arms, are denoted by arrows. This exceptional individual had four gonad arms (three anterior, shown) rather than the two observed in wild-type animals. Scale bars represent 10 μm.

A basic defect in the cytoskeletal organization of *cul-2* embryos is apparent from three phenotypes. First, migration of pronuclei is defective, taking 14 times as long as in wild-type embryos (82 ± 10 min, *n* = 8, versus 5.7 ± 1.5 min, *n* = 10). Second, mitotic spindles are generally mispositioned and misorientated. Third, there are extensive cytoplasmic projections, starting after the first mitotic division, that occur in all directions (Fig. 6a, c–e).

During mitotic embryonic cycles, multiple nuclei of radically different sizes are present in *cul-2* cells (Fig. 6a, b, h, k). The multi-

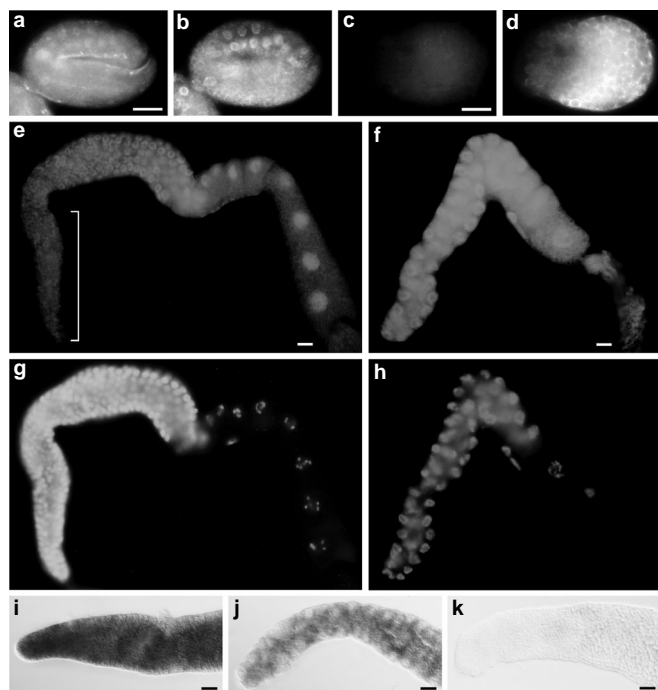


**Figure 5 Level of CKI-1 protein in *cul-2* mutants.** **a–d**, The specificity of the anti-CKI-1 affinity-purified antibody is shown by the absence of specific staining in embryos homozygous for *mnDf100*, a deletion that removes *cki-1*. 12-h-old wild-type (**a, b**) and homozygous *mnDf100* (**c, d**) embryos were stained with affinity-purified anti-CKI-1 antibody (**a, c**) and with an anti-nuclear-pore antibody as a control (**b, d**). We obtained the same staining pattern with anti-CKI-1 antibodies from two different rabbits. **e–h**, Dissected gonad arms from wild-type (**e, g**) and *cul-2(ek1)* (**f, h**) adult hermaphrodites were stained with affinity-purified anti-CKI-1 antibody (**e, f**) and DAPI (**g, h**). In **e**, the bracket indicates the mitotic zone at the distal end. **i, j**, *In situ* hybridization with digoxigenin-labelled *cki-1* antisense probe of wild-type (**i**) and *cul-2* (**j**) adult distal gonads. **k**, Control *in situ* hybridization with *cki-1* sense probe of wild-type adult distal gonad. Scale bars represent 10  $\mu$ m.

nuclei form immediately after cytokinesis (Fig. 6f–h). Mitosis is dramatically lengthened in *cul-2* mutants ( $33 \pm 19$  min for *cul-2* mutants versus  $5.8 \pm 1.5$  min in wild-type embryos;  $n = 33$ ) (Fig. 7). Much of the increase in mitotic length results from an increase in the length of prometaphase. The percentage of *cul-2* cells in prometaphase is increased 1.9-fold relative to wild-type cells, from 35% to 65% ( $n = 100$ ).

**Defect in mitotic chromosome condensation.** During prometaphase, sister chromatids are aligned to the metaphase plate by the mitotic spindle. The mitotic spindle appears normal in *cul-2* embryos (Fig. 8a, c). However, mitotic chromosomes in *cul-2* embryos are strikingly uncondensed (Fig. 8b, d). During anaphase, *cul-2* chromosomes do not segregate cohesively to mitotic poles, and sheared strands of chromosomal DNA are observed (Fig. 8d). The formation of nuclei around missegregated chromosomes and chromosomal fragments apparently contributes to the observed multiple nuclei, some of which have very little DNA (Fig. 6j, k). The following additional defects are attributable to the existence of uncondensed chromosomes: DNA bridges between dividing cells (Fig. 8e, f); unequal DNA segregation (Fig. 6j, k); and failed mitoses, producing cells with multiple centrosomes (Figs 6l–n, 7). Chromosome condensation defects are also observed in the germ line of old *cul-2* adults (4–5 days post-larvae) (data not shown).

To analyse the initial state of mitotic DNA condensation, we observed chromosomes at the beginning of the first prometaphase, immediately after fusion of pronuclei in the zygote. Wild-type

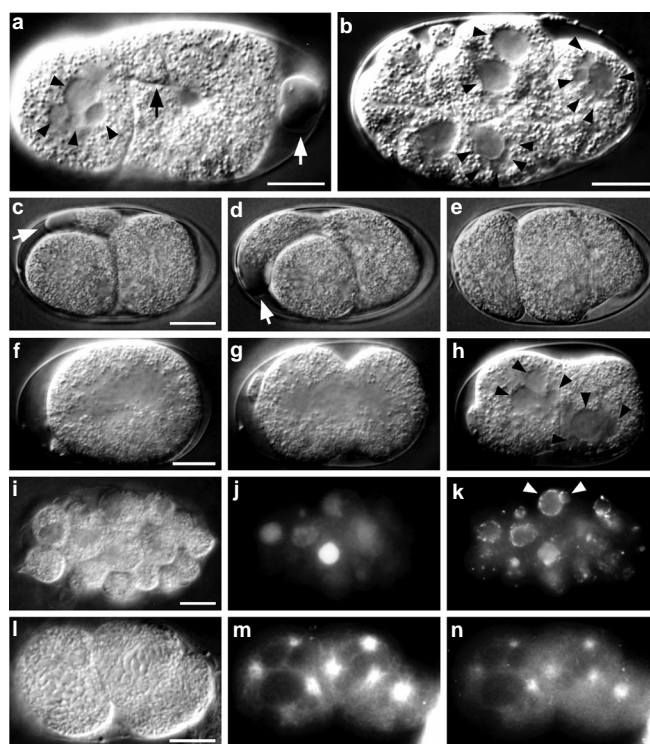


**Figure 6 *cul-2* mutant embryonic phenotype.** Arrowheads indicate multinuclei. **a**, Differential-interference contrast (DIC) micrograph of a *cul-2(ek1)* two-cell-stage embryo. Black and white arrows indicate cytoplasmic extensions of cells situated towards the left and the right of the embryo as pictured, respectively. **b**, DIC micrograph of an embryo from a wild-type parent injected with *cul-2* dsRNA. **c–e**, Cytoplasmic extension creating a cytoplast. Cytoplasmic extensions can retract or form cytoplasts. **c–e** show a time-lapse sequence of DIC micrographs of a *cul-2(ek1)* embryo (total time, <8 min). White arrows indicate cytoplasmic extension. In **e** the cytoplasmic extension has pinched off, creating a cytoplast. **f–h**, Multinuclei in a *cul-2* RNAi embryo. Time-lapse sequence of DIC micrographs of a *cul-2* RNAi embryo undergoing mitosis and cytokinesis. The three micrographs were taken in the span of 17 min. **i–k**, Embryonic-arrest phenotype produced by *cul-2(ek1)*. A *cul-2(ek1)* embryo 12 h after being laid was fixed, observed with DIC (**i**), and stained with  $1 \mu\text{g ml}^{-1}$  DAPI to detect DNA (**j**) and with an anti-nuclear-pore antibody (**k**). Note the unequal DNA distribution among nuclei. **l–n**, Extra centrosomes, resulting from failed mitoses, are present in 59% ( $n = 44$ ) of *cul-2* cells. A *cul-2(ek1)* embryo was observed with DIC (**l**), and stained with anti-tubulin antibody (**m**) and anti-AIR-1 antibody (**n**), which localizes to centrosomes<sup>49</sup>. The two leftward cells each had four centrosomes, three of which are visible for each cell in this focal plane. Scale bars represent 10  $\mu$ m.

zygotes have condensed chromosomes, whereas *cul-2(ek1)* zygotes, including those that show normal meiosis and enter mitosis with the normal 4N content of genomic DNA, have uncondensed chromosomes (Fig. 8g, i; data not shown). At the first mitosis in *cul-2* RNAi embryos, chromosomes enter a prolonged state of partial condensation, presumably because of the effect of residual CUL-2 protein remaining after RNAi (Fig. 8h). Antibody staining revealed that, on average, 2% of CUL-2 protein remains after RNAi, visible upon longer exposure as faint nuclear staining ( $2.0 \pm 2.3$  a.u.,  $n = 10$ , versus wild type,  $100 \pm 57$  a.u.,  $n = 10$ ); *cul-2* mutants show no nuclear staining. In later mitoses, *cul-2* RNAi embryos have chromosomes that are as uncondensed as those in *cul-2(ek1)* embryos (data not shown).

The *cul-2* embryonic phenotype is superficially similar to that of meiosis-defective mutants, such as *mei-1* mutants, which also have multinuclei<sup>26</sup>. To determine whether a failure of meiosis can lead to an inability to condense chromosomes in mitosis, we analysed

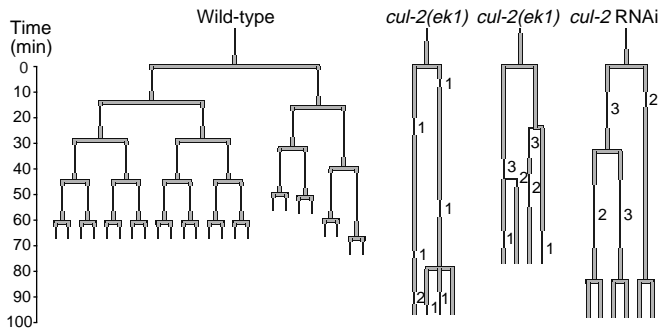


**Figure 7 Cell-cycle lineage of wild-type and *cul-2* mutant embryos.** Left, lineage of a wild-type embryo from cleavage of the zygote to the 24-cell stage. Centre, two representative lineages of *cul-2(ek1)* embryos (from a total of four lineages studied). Right, a representative lineage of a *cul-2* RNAi embryo from an injected wild-type hermaphrodite (from a total of three lineages studied). Horizontal lines denote the time of completion of cytokinesis. The zero time point is set at the cytokinesis that creates the two-cell embryo. Thick vertical lines denote mitosis, as determined by the absence of a nuclear envelope, and thin vertical lines denote interphase. In *cul-2* lineages, numbers on the right side denote the numbers of nuclei per cell; thin lines leaving at a right angle denote a cytoplasm derived from a cytoplasmic extension that had ‘pinched off’ from the main cell; failed mitoses are denoted by an unbranched interphase–mitosis–interphase line.

chromosome condensation in progeny of homozygous *mei-1(b284)* mutants. Multinuclei occur in *mei-1(b284)* mutants when there are excess chromosomes (generally  $\geq 30$ ); however, the chromosomes undergo normal condensation (Fig. 8j). Thus a failure of meiosis does not lead to defects in chromosome condensation.

**Discussion**

We have shown here that *cul-2* is required in *C. elegans* germ cells for the G1-to-S-phase transition. The *cul-2* G1 arrest is correlated with increased levels of CKI-1. *cul-2* is also required for proper cytoskeletal movement and mitotic chromosome condensation in early embryos, which lack a G1 phase<sup>27</sup>. *cul-2* is expressed specifically in dividing larval cells. It is not yet known whether somatic larval *cul-2* mutant phenotypes are masked by *cul-2* maternal product. Germ cells, which divide substantially more than other tissues, undergo a G1 arrest only in later larval stages, indicating that *cul-2* maternal product may be diluted to non-functional levels only after extensive proliferation.

The observation that mitotic chromosome condensation requires CUL-2, a ubiquitin-ligase component, indicates that ubiquitin-mediated proteolysis may be required for this process *in vivo*. It is not known at present how CUL-2 facilitates chromosome condensation. The phosphorylation of histone H3 on mitosis-specific sites is an early event that is required for proper condensation<sup>28,29</sup>. In *cul-2* embryos this phosphorylation is still observed, so *cul-2* is not required for this process (data not shown).

SCF complexes function in both G1 and G2/M phases. *cdc34* or *cdc53* mutants in the absence of the CKI Sic1 undergo a G2 or mitotic arrest<sup>6</sup>. In contrast, *cul-2* mutant cells complete mitosis, often producing ‘cut’ phenotypes similar to that observed in yeast condensin mutants defective in chromosome condensation<sup>30</sup> (Fig. 8e). *Cdc34* and *Cdc53* are required for the degradation of the Swe1/Wee1 CDK-inhibitory kinase, which negatively regulates entry into mitosis<sup>4,5</sup>. However, it is unlikely that *cul-2* is required for the degradation of Wee1, as a failure to degrade Wee1 would lead to a failure to activate the mitotic CDK, CDK1, and CDK1 activation appears to be unaffected in *cul-2* mutants: nuclear-envelope breakdown and the assembly of the mitotic spindle, both of which require CDK1 activity<sup>31</sup>, occur normally.

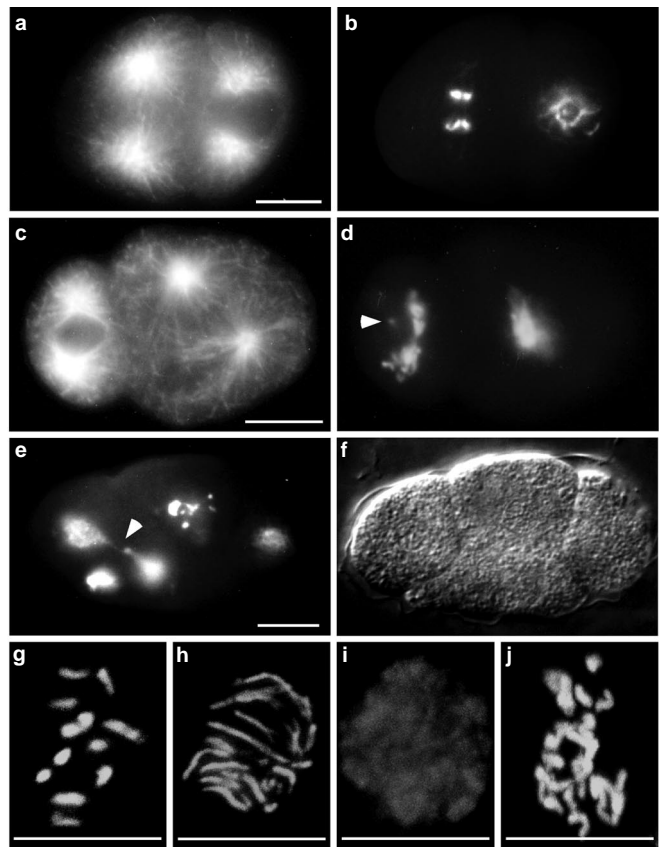


**Figure 8 Chromosome condensation is impaired in *cul-2* mutant embryos.** **a–d**, Anaphase in *cul-2* and wild-type two-cell-stage embryos. Wild-type (**a, b**) and *cul-2(ek1)* (**c, d**) two-cell stage embryos were fixed and stained with anti-tubulin antibody (**a, c**) and DAPI (**b, d**). **a, b**, In the wild type, the left-hand cell, P<sub>1</sub>, is in anaphase while the right-hand cell, P<sub>2</sub>, is in prophase. **c, d**, In *cul-2(ek1)* embryos, the left-hand cell is in anaphase, while the right-hand cell is in prometaphase. The arrowhead in **d** indicates a chromosomal fragment that is not segregated with the rest of the chromosomes. **e, f**, DNA bridge in a *cul-2(ek1)* mutant. A fixed *cul-2(ek1)* embryo was stained with DAPI (**e**) and observed by differential-interference contrast (DIC) microscopy (**f**). The DNA bridge in **e** is marked by arrowhead. **g, i, j**, Genomic DNA from wild-type (**g**), *cul-2(ek1)* (**i**) and *mei-1(b284)* (**j**) zygotes that were fixed immediately upon fusion of maternal and paternal pronuclei and then stained with propidium iodide to visualize DNA. A projection of the three-dimensional confocal serial sections was collapsed into two dimensions. Note that several of the 30 *mei-1(b284)* chromosomes overlap because of the projection of the three-dimensional sections onto two dimensions. **h**, Confocal projection of propidium-iodide-stained genomic DNA from a *cul-2* RNAi zygote that was fixed 5 min after fusion of maternal and paternal pronuclei. Note that wild-type embryos complete mitosis within 5 min. The projections in **g–j** are representative of 23, 17, 8 and 10 pronuclear fusions studied, respectively. Scale bars represent 10  $\mu$ m.

Overexpression of CKI-1 inhibits cell division<sup>25</sup>. In *cul-2* germ cells, there is a post-transcriptional increase in the level of CKI-1 that correlates with the G1-arrest phenotype. Thus, CUL-2 may function as an E3 to target CKI-1 for degradation. A second *C. elegans* CIP/KIP family member, CKI-2, does not show increased protein levels in *cul-2* mutants, and does not appear from RNAi studies to function as a negative cell-cycle regulator.

Human CUL-2 has been found in a complex containing VHL, Elongins B and C, and RBX1/ROC1 (refs 9, 18, 19). *C. elegans cul-2* and human VHL produce opposite mutant phenotypes, namely G1 arrest and tumour formation, respectively. This indicates that human CUL-2 may have cellular functions that are independent of VHL. It has been proposed that different substrate-binding adaptor

proteins (besides VHL) bind the CUL-2/Elongin-C/Elongin-B/RBX1 complex<sup>32–34</sup>. One can envision a model in which VHL competes with other adaptors for CUL-2 binding, thereby sequestering CUL-2 from an E3 complex(es) that is required for CKI degradation. In the absence of VHL, CUL-2 would form more of the E3 complex(es) that functions to reduce the levels of CKIs, thereby potentiating hyperplasia. In support of this model, it has been observed that mammalian cells lacking VHL are unable to exit the cell cycle upon serum withdrawal, and this failure is correlated with an inability to accumulate the CKI p27<sup>KIP1</sup> (ref. 35). Conversely, overexpression of VHL produces a G1 arrest with an increased level of p27<sup>KIP1</sup> (ref. 36). Human SKP2 in combination with CUL-1 has been found to target p27<sup>KIP1</sup> for degradation *in vitro* and upon overexpression *in vivo*<sup>37–39</sup>; however, there appear to be SKP2- and CUL-1-independent pathways for p27<sup>KIP1</sup> degradation, as inactivation of SKP2 or CUL-1 in certain cell lines has no effect on p27<sup>KIP1</sup> levels<sup>40</sup>. Further studies will be required to determine whether CUL-2 is required to negatively regulate CKI levels in humans, and whether the presence or absence of VHL alters human CUL-2 activity. □

## Methods

### C. elegans observation and genetics.

Embryonic lineages were followed with a Zeiss Axioscope microscope and recorded with an Optronics charge-coupled-device (CCD) camera feeding images into a Panasonic AG-6740 time-lapse VCR. Cell-cycle events in the fertilized oocyte were observed in the adult hermaphrodite's body by immobilizing animals with 0.1% tricaine and 0.01% tetramisole (Sigma) as described<sup>41</sup>. Cell number in embryos was determined by fixing embryos in methanol and acetone (10 min each), staining DNA with propidium iodide, and observing nuclei in serial sections from a confocal microscope. To observe *cul-1*, *cul-2* double homozygotes, we created a strain with *cul-1* and *cul-2* in *cis* balanced by a deficiency located between the genes, strain *cul-1(e1756) cul-2(ek1)eDj2*.

### RNA interference.

RNA was synthesized from linearized plasmids containing the full-length clones of *cul-2*, *cki-1* and *cki-2* with either the T3 or the T7 MegaScript Kit (Ambion) to produce sense or antisense RNA transcripts, respectively. Equal amounts of sense and antisense RNA were annealed to create dsRNA by incubation at 95°C for 5 min and then at 70°C for 20 min. dsRNA was injected into the distal gonad arms of young wild-type adults at a concentration of 0.5–1 mg ml<sup>-1</sup>. For suppression of the *cul-2(ek1)* phenotype by injection of *cki* dsRNA, L4 hermaphrodites were injected in their intestines with dsRNA at 0.5–1.0 mg ml<sup>-1</sup>.

### Isolation of *cul-2* deletion mutant.

The deletion screen was based on an outline presented by Johnson<sup>41</sup>. Synchronized L4 animals<sup>17</sup> were mutagenized with 50 mM ethylmethanesulphonate for 4 h. Eggs from the mutagenized animals were collected by treatment with hypochlorite. The F<sub>1</sub> progeny were seeded at 20 animals per well in a 96-well plate in NGM media supplemented with OP50 bacteria. Ninety-six 96-well plates were created, to produce a library of 370,000 mutagenized genomes. Half of the F<sub>2</sub> progeny were frozen and half were used to make DNA<sup>42</sup>. Two rounds of nested polymerase chain reactions (PCRs) were performed on pooled DNA from each 96-well plate, using primer pairs separated by 4.5 kilobases of genomic sequence. Wells containing deletion bands were identified by PCR of row and column DNA from the 96-well plates. Animals were recovered from the frozen well and cloned. Single-worm PCR was performed on animals after they had produced progeny, to identify animals containing the *cul-2* mutation. The mutant allele, *ek1*, was outcrossed six times and balanced with *unc-64(e264)*. The site of deletion was determined by sequencing PCR products.

### Isolation of *cki* complementary DNAs.

The *cki-1* and *cki-2* genes were identified by homology searches of the *C. elegans* genome database<sup>43</sup>. The 3' sequences of *cki-1* and *cki-2* were obtained by sequencing complementary DNA clones obtained from the *C. elegans* expressed-sequence tag (EST) project, namely clones yk490e9 and yk374f4, respectively. The 5' ends of both genes were cloned by PCR from a cDNA library by using internal primers and a 5' primer corresponding to the *trans*-spliced leader SL1 (ref. 44). The presence of SL1 indicates that both clones are full length. Phylogenetic analysis was performed by aligning CKI proteins with the clustalW sequence-alignment program<sup>45</sup>. The most parsimonious tree (Fig. 4c) was obtained with the exhaustive search method using the PAUP parsimony programme<sup>46</sup>.

### Antibody production, immunofluorescence and *in situ* hybridization.

Antisera to full-length CKI-1, CUL-2 and the amino-terminal 135 amino acids of CKI-2 were produced in rabbits using bacterially derived histidine-tagged fusion proteins as antigens (vector pET32a+, Novagen). Fusion proteins were isolated under denaturing conditions using Ni-NTA agarose (Qiagen) according to the manufacturer's instructions. Sera were precleared of anti-histidine-tag antibodies by passage over Affigel-10 (BioRad) linked to histidine tag, and then affinity-purified against the antigen linked to Affigel-15, as described<sup>47</sup>.

Embryos were obtained by hypochlorite treatment and frozen on poly-lysine-coated slides. Gonad arms were dissected from adult hermaphrodites by placing animals in M9 solution on a poly-lysine-coated slide and cutting the animals behind the pharynx so that the extruded gonads attached to the slide. Slides were processed using the 'freeze-crack' method, followed by methanol and acetone fixation (30 min at -20°C for each), and probed with primary and secondary antibodies as described<sup>48</sup>.

The following primary antibodies were also used: anti-nuclear-pore monoclonal antibody MAb414 (Babco); anti- $\alpha$ -tubulin monoclonal antibody N356 (Amersham); anti-histone monoclonal antibody

MAB052 (Chemicon International); polyclonal antibody against AIR-1, a centrosome marker<sup>49</sup>; and polyclonal antibody against phosphorylated histone H3, a mitotic marker<sup>28</sup> (Upstate Biotechnology). The secondary antibodies used were goat anti-mouse conjugated to rhodamine (Cappel) or fluorescein isothiocyanate (FITC), and goat anti-rabbit conjugated to rhodamine or FITC (all from Boehringer Mannheim). Secondary antibodies were precleared with acetone-fixed *C. elegans* powder as described<sup>48</sup>.

To determine the percentage of cells in the various mitotic stages, we stained wild-type and *cul-2(ek1)* embryos with anti-phospho-histone H3 antibody<sup>28</sup>, anti-AIR-1 antibody<sup>49</sup> and 4,6-diamidino-2-phenylindole (DAPI). Only cells with two centrosomes were analysed.

Antisense and sense digoxigenin-labelled RNA probes were created from full-length *cul-2* and *cki-1* cDNAs using digoxigenin-11-UTP (Boehringer Mannheim) according to the manufacturer's protocol. Whole animals and dissected gonad arms were frozen immediately beneath a coverslip and processed for *in situ* hybridization as described<sup>48</sup>, except that the hybridization and washes were at 55 °C.

### Microscopy and signal quantification.

Germ-cell DNA levels were quantified in young adult hermaphrodites that were fixed using the 'freeze-crack' method described above. Fixed specimens were incubated with 40  $\mu$ g ml<sup>-1</sup> RNase A in PBS for 1 h at 37°C, stained with 50  $\mu$ g ml<sup>-1</sup> propidium iodide (Sigma) for 30 min at room temperature, and then rinsed with PBS. Specimens were mounted in 1 mg ml<sup>-1</sup> *p*-phenylenediamine in 90% glycerol and observed with an MRC600 Biorad confocal microscope. Germ cells within five cell diameters from the distal tip cell were serially scanned. The same confocal settings were used for all specimens of a given experiment and set so that no image saturated. A  $\times 100$  objective was used with a scan depth of 0.5  $\mu$ m. Quantification was accomplished with Comos software version 7.0 (Biorad). The signal from nuclei in a given slice was determined by multiplying the average intensity for the nuclei (minus background intensity) by the area. The total signal from nuclei was obtained by adding the signal from serial sections. DNA content was normalized to haploid genome equivalents by using the DNA content from somatic cells, other than hypodermis or intestine, as internal 2N standards; mitotic germ cells were used as internal 4N standards. Quantification of protein levels in gonad arms was accomplished by dissection of *cul-2* and wild-type gonad arms on the same slide and processing for immunofluorescence with polyclonal and anti-nuclear-pore antibody. Quantification was as above.

Microscope images were captured on TechPan film (Kodak) and digitally scanned with a Nikon LS-2000 scanner. The images were processed with Adobe Photoshop version 4.0. For matched images, such as CKI-1 level in *cul-2* and wild-type animals, the same shutter time (in seconds) was used and the images were processed identically.

RECEIVED 12 MAY 1999; REVISED 23 SEPTEMBER 1999; ACCEPTED 18 OCTOBER 1999; PUBLISHED 2 NOVEMBER 1999.

- Pines, J. Cyclins and cyclin-dependent kinases: a biochemical view. *Biochem. J.* **308**, 697–711 (1995).
- Hershko, A. & Ciechanover, A. The ubiquitin system. *Annu. Rev. Biochem.* **67**, 425–479 (1998).
- Peters, J.-M. SCF and APC: the Yin and Yang of cell cycle regulated proteolysis. *Curr. Opin. Cell Biol.* **10**, 759–768 (1998).
- Michael, W. M. & Newport, J. Coupling of mitosis to the completion of S phase through Cdc34-mediated degradation of Wee1. *Science* **282**, 1886–1889 (1998).
- Kaiser, P., Sia, R. A. L., Bardes, E. G. S., Lew, D. J. & Reed, S. I. Cdc34 and the F-box protein Met30 are required for degradation of the cdk-inhibitory kinase Swe1. *Genes Dev.* **12**, 2587–2597 (1998).
- Schwob, E., Bohm, T., Mendenhall, M. D. & Nasmith, K. The B-type cyclin kinase inhibitor p40<sup>SC1</sup> controls the G1 to S transition in *S. cerevisiae*. *Cell* **79**, 233–244 (1994).
- Feldman, R. M. R., Correll, C. C., Kaplan, K. B. & Deshaies, R. J. A complex of Cdc4p, Skp1p, and Cdc53p/Cullin catalyzes ubiquitination of the phosphorylated CDK inhibitor Sic1p. *Cell* **91**, 221–230 (1997).
- Skowrya, D., Craig, K. L., Tyers, M., Elledge, S. J. & Harper, J. W. F-Box proteins are receptors that recruit phosphorylated substrates to the SCF ubiquitin-ligase complex. *Cell* **91**, 209–219 (1997).
- Kamura, T. *et al.* Rbx1, a component of the VHL tumor suppressor complex and SCF ubiquitin ligase. *Science* **284**, 657–661 (1999).
- Skowrya, D. *et al.* Reconstitution of G1 cyclin ubiquitination with complexes containing SCFGrr1 and Rbx1. *Science* **284**, 662–665 (1999).
- Ohta, T., Michel, J. J., Schottelius, A. J. & Xiong, Y. ROC1, a homolog of APC11, represents a family of cullin partners with an associated ubiquitin ligase activity. *Mol. Cell* **3**, 535–541 (1999).
- Tan, P. *et al.* Recruitment of a ROC1-CUL1 ubiquitin ligase by Skp1 and HOS to catalyze the ubiquitination of Ikb $\alpha$ . *Mol. Cell* **3**, 527–533 (1999).
- Bai, C. *et al.* SKP1 connects cell cycle regulators to the ubiquitin proteolysis machinery through a novel motif, the F-box. *Cell* **86**, 263–274 (1996).
- Deshaies, R. J., Chau, V. & Kirschner, M. Ubiquitination of the G1 cyclin Cln2p by a Cdc34p-dependent pathway. *EMBO J.* **14**, 303–312 (1995).
- Willems, A. R. *et al.* Cdc53 targets phosphorylated G1 cyclins for degradation by the ubiquitin proteolytic pathway. *Cell* **86**, 453–463 (1996).
- Henchoz, S. *et al.* Phosphorylation- and ubiquitin-dependent degradation of the cyclin-dependent kinase inhibitor Far1p in budding yeast. *Genes Dev.* **11**, 3046–3060 (1997).
- Kipreos, E. T., Lander, L. E., Wing, J. P., He, W. W. & Hedgecock, E. M. *cul-1* is required for cell cycle exit in *C. elegans* and identifies a novel gene family. *Cell* **85**, 829–839 (1996).
- Pause, A. *et al.* The von Hippel-Lindau tumor-suppressor gene product forms a stable complex with human CUL-2, a member of the Cdc53 family of proteins. *Proc. Natl. Acad. Sci. USA* **94**, 2155–2161 (1997).
- Lonergan, K. M. *et al.* Regulation of hypoxia-inducible mRNAs by the von Hippel-Lindau tumor suppressor protein requires binding to complexes containing Elongins B/C and Cul2. *Mol. Cell Biol.* **18**, 732–741 (1998).
- Lisztwan, J., Imbert, G., Wirbelauer, C., Gstaiger, M. & Krek, W. The von Hippel-Lindau tumor suppressor protein is a component of an E3 ubiquitin-protein ligase activity. *Genes Dev.* **13**, 1822–1833 (1999).
- Maxwell, P. H. *et al.* The tumour suppressor protein VHL targets hypoxia-inducible factors for oxygen-dependent proteolysis. *Nature* **399**, 271–275 (1999).
- Kaelin, W. G. & Maher, E. R. The VHL tumour-suppressor gene paradigm. *Trends Genet.* **14**, 423–426 (1998).
- Hedgecock, E. M. & White, J. G. Polyploid tissues in the nematode *Caenorhabditis elegans*. *Dev. Biol.*

- 107, 128–133 (1985).
24. Fire, A. *et al.* Potent and specific genetic interference by double-stranded RNA in *Caenorhabditis elegans*. *Nature* 391, 806–811 (1998).
  25. Hong, G., Roy, R. & Ambros, V. Developmental regulation of a cyclin-dependent kinase inhibitor controls postembryonic cell cycle progression in *C. elegans*. *Development* 125, 3585–3597 (1998).
  26. Mains, P. E., Kempfues, K. J., Sprunger, S. A., Sulston, I. A. & Wood, W. B. Mutations affecting the meiotic and mitotic divisions of the early *Caenorhabditis elegans* embryo. *Genetics* 126, 593–605 (1990).
  27. Edgar, L. G. & McGhee, J. D. DNA synthesis and the control of embryonic gene expression in *C. elegans*. *Cell* 53, 589–599 (1988).
  28. Hendzel, M. J. *et al.* Mitosis-specific phosphorylation of histone H3 initiates primarily within pericentromeric heterochromatin during G2 and spreads in an ordered fashion coincident with mitotic chromosome condensation. *Chromosoma* 106, 348–360 (1997).
  29. Wei, Y., Yu, L., Bowen, J., Gorovsky, M. A. & Allis, C. D. Phosphorylation of histone H3 is required for proper chromosome condensation and segregation. *Cell* 97, 99–109 (1999).
  30. Koshland, D. & Strunnikov, A. Mitotic chromosome condensation. *Annu. Rev. Cell Dev. Biol.* 12, 305–333 (1996).
  31. Boxem, M., Srinivasan, D. G. & van den Heuvel, S. The *Caenorhabditis elegans* gene *ncc-1* encodes a cdc2-related kinase required for M phase in meiotic and mitotic cell divisions, but not for S phase. *Development* 126, 2227–2239 (1999).
  32. Stebbins, C. E., Kaelin, W. G. & Pavletich, N. P. Structure of the VHL-ElonginC-ElonginB complex: implications for VHL tumor suppressor function. *Science* 284, 455–461 (1999).
  33. Kamura, T. *et al.* The elongin BC complex interacts with the conserved SOCS-box motif present in members of the SOCS, ras, WD-40 repeat, and ankyrin repeat families. *Genes Dev.* 12, 3872–3881 (1998).
  34. Zhang, J.-G. *et al.* The conserved SOCS box motif in suppressors of cytokine signaling binds to elongins B and C and may couple bound proteins to proteasomal degradation. *Proc. Natl Acad. Sci. USA* 96, 2071–2076 (1999).
  35. Pause, A., Lee, S., Lonergan, K. M. & Klausner, R. D. The von Hippel-Lindau tumor suppressor gene is required for cell cycle exit upon serum withdrawal. *Proc. Natl Acad. Sci. USA* 95, 993–998 (1998).
  36. Kim, M. *et al.* Recombinant adenovirus expressing Von Hippel-Lindau-mediated cell cycle arrest is associated with the induction of cyclin-dependent kinase inhibitor p27<sup>Kip1</sup>. *Biochem. Biophys. Res. Comm.* 253, 672–677 (1998).
  37. Carrano, A. C., Eytan, E., Hershko, A. & Pagano, M. SKP2 is required for ubiquitin-mediated degradation of the CDK inhibitor p27. *Nature Cell Biol.* 1, 193–199 (1999).
  38. Sutterluty, H. *et al.* p45<sup>SKP2</sup> promotes p27<sup>Kip1</sup> degradation and induces S phase in quiescent cells. *Nature Cell Biol.* 1, 207–214 (1999).
  39. Tsvetkov, L. M., Yeh, K.-H., Lee, S.-J., Sun, H. & Zhang, H. p27<sup>Kip1</sup> ubiquitination and degradation is regulated by the SCF<sup>SKP2</sup> complex through phosphorylated Thr187 in p27. *Curr. Biol.* 9, 661–664 (1999).
  40. Yu, Z.-K., Gervais, J. L. M. & Zhang, H. Human CUL-1 associates with the SKP1/SKP2 complex and regulates p21<sup>CIP1/WAF1</sup> and cyclin D proteins. *Proc. Natl Acad. Sci. USA* 95, 11324–11329 (1998).
  41. Kirby, C., Kusch, M. & Kempfues, K. Mutation in the *par* genes of *Caenorhabditis elegans* affect cytoplasmic reorganization during the first cell cycle. *Dev. Biol.* 142, 203–215 (1990).
  42. Plasterk, R. H. A. in *Caenorhabditis elegans: Modern Biological Analysis of an Organism. Methods in Cell Biology* Vol. 48 (eds Epstein, H. F. & Shakes, D. C.) 59–80 (Academic, San Diego, 1995).
  43. The *C. elegans* Sequencing Consortium. Genome sequence of the nematode *C. elegans*: a platform for investigating biology. *Science* 282, 2012–2018 (1998).
  44. Krause, M. & Hirsh, D. A trans-spliced leader on actin mRNA in *C. elegans*. *Cell* 49, 753–761 (1987).
  45. Thompson, J. D., Higgins, D. G. & Gibson, T. J. CLUSTAL W: improving the sensitivity of progressive multiple sequence alignment through sequence weighting, positions-specific gap penalties and weight matrix choice. *Nucleic Acids Res.* 22, 4673–4680 (1994).
  46. Swofford, D. L. PAUP: *Phylogenetic Analysis Using Parsimony* Version 3.1. (Illinois Nat. Hist. Survey, Champaign, IL, 1993).
  47. Harlow, E. & Lane, D. *Antibodies (A Laboratory Manual)* (Cold Spring Harb. Lab., Cold Spring Harb., NY, 1988).
  48. Miller, D. M. & Shakes, D. C. in *Caenorhabditis elegans: Modern Biological Analysis of an Organism. Methods in Cell Biology* Vol. 48 (eds Epstein, H. F. & Shakes, D. C.) 365–394 (Academic, San Diego, 1995).
  49. Schumacher, J. M., Ashcroft, N., Donovan, P. J. & Golden, A. A highly conserved centrosomal kinase, AIR-1, is required for accurate cell cycle progression and segregation of developmental factors in *Caenorhabditis elegans* embryos. *Development* 125, 4391–4402 (1998).
  50. Seydoux, G. & Fire, A. in *Caenorhabditis elegans: Modern Biological Analysis of an Organism. Methods in Cell Biology* Vol. 48 (eds Epstein, H. F. & Shakes, D. C.) 323–339 (Academic, San Diego, 1995).
  51. Johnson, C. at 11th International *C. elegans* meeting May 28–June 1, 1997 (Univ. Wisconsin, Madison, WI, USA).

ACKNOWLEDGEMENTS

We thank the *Caenorhabditis* Genetics Center for *C. elegans* strains; Y. Kohara for cDNA clones; A. Golden for anti-AIR-1 antibody; R.J. Barstead for a cDNA library; M. Farmer, M. Fechtmeier, P. Shen and H. Cai for technical advice; V. Ambros and J. Rothman for communicating results before publication; the Genome Sequencing Consortium for *C. elegans* genomic sequence and cosmids; T. Schedl for helpful discussions; C. Johnson and L. Liu for providing a second *cul-2* deletion allele, which produced an identical phenotype to that produced by allele *ek1*; and M. Pagano, G. Seydoux and C. Norris for critical reading of the manuscript. This project was supported by NIH grant R01 GM55297 and HFSP grant RG-229/98 (to E.T.K.). Correspondence and requests for materials should be addressed to E.T.K. The *cki-1* and *cki-2* cDNA sequences have been deposited at GenBank under accession numbers AF179358 and AF179359, respectively.